AIAA JOURNAL
Vol. 39, No. 10, October 2001

Intelligent Computational Methods for Corrosion Damage Assessment

M. J. Palakal,* R. M. V. Pidaparti,† and S. Rebbapragada‡
Indiana University, Indianapolis, Indiana 46202
and
C. R. Jones§
Sandia National Laboratories, Albuquerque, New Mexico 87106

Corrosion is one of the damage mechanisms affecting the structural integrity of aging aircraft structures. Various nondestructive inspection (NDI) techniques are being used to obtain images of corroded regions on structures. A computational approach using wavelet transforms and artificial neural networks to analyze and quantify the extent of corrosion damage from the NDI images is described. The wavelet parameters obtained from the images were first used to classify between corroded and uncorroded regions using a clustering algorithm. The corroded regions were further analyzed to obtain the material loss due to corrosion using an artificial neural network model. Experiments were carried out to investigate the developed methods for aircraft panels with engineered corrosion obtained from the Federal Aviation Administration Validation Center in Albuquerque. The results presented indicate that the computational methods developed for corrosion analysis seem to provide reasonable results for estimating material loss due to corrosion damage.

I. Introduction

CORROSION is one of the damage mechanisms affecting the structural integrity of aging aircraft. Structural damage may also be due to fatigue and/or wear of the material resulting from operating conditions and the environment. To better understand corrosion mechanisms in aircraft aluminum alloys, optical microscopy, scanning electron microscopy, and transmission electron microscopy techniques have been used. In addition, a number of nondestructive techniques such as eddy current, thermal imaging, acoustic emission, ultrasound, etc., are currently used to obtain image of corroded structures.

Nondestructive evaluation (NDE) procedures involve establishing correlations between measured properties and quantitative information about anomalies. For example, eddy current NDE involves measurement of impedance and correlating it with the damage (crack or change in material or microstructure) producing it. There is a growing demand for improving existing NDE techniques to achieve maximum confidence and reliable results with minimum damage components. Also, because of damage tolerance requirements, detecting and quantifying even the smallest damage is required. Manual identification and quantification of the damages on NDI images is a tedious and subjective task. With automatic identification and quantification of damaged regions, maintenance personnel can schedule regular service inspections more economically without compromising safety requirements.

Conventional nondestructive inspection (NDI) techniques using signals from ultrasound and eddy current methods contribute to poor signal-to-noise ratio and interfere with the damage signals. Further, it is not possible to determine parameters such as thickness or the morphological properties of the damage. This poses a problem for accurate characterization and quantification of damage due to corrosion and widespread fatigue in aging aircraft. On the other hand, two-dimensional signals or images obtained using NDI techniques such as infrared imaging, ultrasonic C-scan imaging, scanning acoustic microscopy, eddy current imaging, etc., can be effectively used to assess the damage more accurately. However, because of noise in the signal, the images obtained through these methods may distort images of the damaged regions. Therefore, improved image enhancement methods may contribute to increased accuracy in detection and cost effectiveness for the damage identification and quantification processes. Signal processing and the use of pattern recognition techniques have been applied to NDE problems since the 1970s. Some early examples of pattern recognition in NDE using eddy current and acoustic emission signals are given in Refs. 1–4. A few NDE systems have been developed that incorporate pattern recognition and artificial intelligence techniques such as interactive ultrasonic NDE,[5] ICEPAK,[6] and TestPro.[7]

Spectral analysis, deconvolution, and time-frequency analysis are the three main approaches based on signal processing in NDE.[8] Modern spectral analysis makes it possible to determine a high resolution and a reliable spectrum. However, the problem is the lack of quantitative relationship available to calculate defect parameters from the spectrum.[8] Deconvolution can be used for thickness and depth measurements; however, it is difficult to determine other parameters such as size and shape of a defect from the impulse response.

The short-term Fourier analysis, Weigner distribution, and the wavelet transform are most often used in time-frequency analysis. Both the wavelet transform and Weigner distribution are also useful to extract features for ultrasonic signal classification (unpublished report submitted to the U.S. Army Material Technology Laboratory by Chen, C. H., and Lee, G. G., "On Wavelet Transform and Its Application to Ultrasonic NDE," June 1992). The reported work on time-frequency analysis has been very limited, and this is a research topic that remains to be explored.[8] Neural networks have been proven to be very effective for eddy signal classification using Fourier descriptors as features.[9]

In this paper, we specially address the analysis of one type of damage that appears on most structures, that is, corrosion. Corroded regions appear as changes in texture on the material, and it occurss due to operational conditions to which the material is exposed. Corrosion identification and analysis can be considered as texture analysis process, which is a well-studied problem in the field of artificial intelligence and pattern recognition. Texture analysis methods developed through these studies has been effectively applied in automated inspection problems, medical image analysis, document processing, and remote sensing.[10]

Received 3 July 2000; revision received 15 January 2001; accepted for publication 22 February 2001. Copyright © 2001 by the American Institute of Aeronautics and Astronautics, Inc. All rights reserved.

*Associate Professor, Department of Computer and Information Science, 723 W. Michigan Street, SL 280.
†Professor, Department of Mechanical Engineering, 723 W. Michigan Street, SL 260. Associate Fellow AIAA.
‡Graduate Student, Department of Computer Science.
§Senior Technical Staff, Federal Aviation Administration–Nondestruction Inspection Validation Center.

Recently, Levens[11] used the wavelets for corrosion analysis based on texture properties. In the experiments conducted, various corrosion images were classified into two morphologies: pit formation and cracking. The images were not segmented, and the damaged regions were not identified for further analysis and quantification. In this paper we attempt to bridge these shortcomings by developing computational methods to quantify the corrosion damage in aircraft panels. Section II of this paper presents the overall process that involves analyzing and estimating the material loss based on NDI images of corrosion. Section III describes in detail the computational aspects of detecting corroded regions in the images. The damage quantification, that is, estimation of material loss, is discussed in Sec. IV. Experimental results using the data obtained from Federal Aviation Administration (FAA) NDI Validation Center in New Mexico is given in Sec. V.

II. Corrosion Detection and Quantification Process

The overall process of identification and quantification of corroded regions from NDI images is shown in Figs. 1 and 2. The process essentially involves two stages: first, classification of various regions in the image as corroded or uncorroded and, second, prediction of the material loss of the corroded regions. The classification process involves segmenting the image into various regions. Multiresolution wavelet analysis is performed on the NDI images to obtain a set of wavelet coefficients as feature vectors. These features were used for the identification of the damaged regions on the NDI images using clustering techniques. Each of the segments on the segmented image would correspond to a damaged region or an undamaged region. Segmentation of the images of damaged panels is similar to the segmentation of texture images. Though a number of segmentation algorithms are available in the literature, texture segmentation based on wavelets is considered a powerful technique. After the image is segmented, histogram features are extracted from each segment.

After the damaged segments are identified, a number of features are extracted from each identified segment and a backpropagation neural network is used to quantify the damage. Neural networks are capable of realizing a variety of nonlinear relationships of considerable complexity and are effectively used in this research.[12] The quantification of damage is based on the extent of material loss.

A number of experiments were conducted by perturbing the images in the direction of growth in corrosion and also by changing the number of features used in the quantification of damage. The images obtained using the NDI techniques depend on the devising technique, its frequency, and the specimen. Material loss prediction experiments were conducted on a set of NDI images on different specimens. The results are compared to actual experimental data to demonstrate the present approach to quantify the corrosion damage in aircraft structures. The process of damage identification and quantification are provided in the following sections.

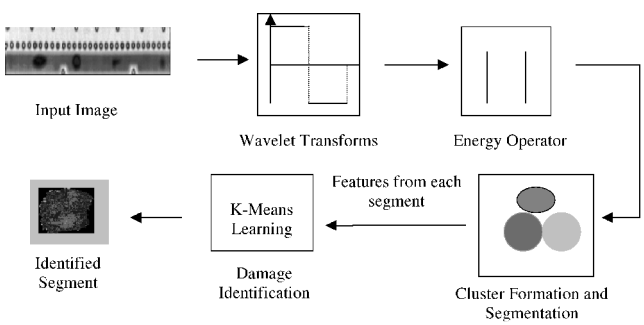

Fig. 1 Schematic of the process used to identify the damaged regions on an NDI image.

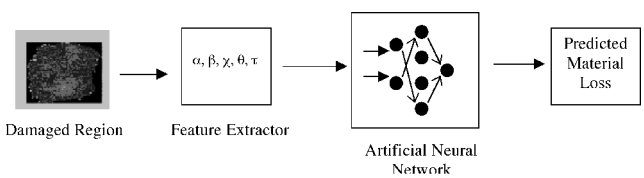

Fig. 2 Schematic of the process used to quantify the material loss on a damaged region.

III. Damage Identification

The images that are obtained through conventional NDI methods are not directly suitable for identification of damaged regions automatically. Therefore, the damage identification process involves three major steps: feature extraction, segmentation, and classification. As shown in Fig. 1, wavelet analysis techniques are used for feature extraction, a clustering technique is used for segmentation, and K-means distance-based method is used for damage classification. Image segmentation is an important step in this whole process. The segmentation process essentially identifies various regions in a given image. Traditionally, segmentation algorithms are based on one of the two basic properties of gray-level values: discontinuity and similarity. These methods are usually classified as thresholding, edge detection or gradient based, region growing, and hierarchical schemes.[13] Feature extraction is an important step in accomplishing segmentation. Most of the traditional texture analysis algorithms rely on statistical approaches, and their performance is limited to a class of so-called microtextures.[14] In the past decade, combined spatial/frequency representations, which provide localized frequency information, particularly the use of wavelet analysis, have found wide use in the field of texture analysis.[15–17] These techniques are effectively used in the segmentation of NDI images.

The problem of texture analysis is broadly classified into four categories: texture segmentation, texture classification, texture synthesis, and shape recognition[18] In our application analyzing corrosion, texture segmentation and classification are the two problems that are considered. Texture analysis uses various mathematical approaches such as statistical,[19] geometrical,[20] model-based,[21,22] and signal processing[23] methods. In this paper, we show how wavelet[24] features, one form of signal processing method, can be used for texture segmentation and for estimating the material loss due to corrosion.

Segmentation Based on Wavelets

An image can be considered as a two-dimensional signal. A number of techniques are available to analyze/process a signal. Fourier analysis is probably the most well known. It breaks down a signal into constituent sinusoids of different frequencies. A two-dimensional discrete Fourier transformation of an $N \times N$ image can be given by

$$F(u, v) = \frac{1}{N} \sum_{r=0}^{N-1} \sum_{c=0}^{N-1} I(r, c) \exp\left[-j2\pi \left(\frac{ur + vc}{N}\right)\right] \quad (1)$$

$F(u,v)$ is a complex number with the real part corresponding to the cosine terms and the imaginary part corresponding to the sine terms and can, therefore, be represented as $F(u, v) = R(u, v) + jI(u, v)$. The magnitude and phase of the complex can be defined as

$$\text{magnitude} = |F(u, v)| = \sqrt{\{[R(u, v)]^2 + [I(u, v)]^2\}}$$

$$\text{phase} = \phi(u, v) = \tan^{-1}\left[\frac{I(u, v)}{R(u, v)}\right] \quad (2)$$

One of the serious drawbacks of Fourier transformations is that it loses the spatial (time) information. For example, when the Fourier transform of an image is looked at, it is impossible to tell where (when) a particular event took place.

Gabor adapted the Fourier transform by analyzing only a small section of the signal at a time, a technique called windowing the signal. Gabor's adaptation, called short-time Fourier transforms (STFT), maps a signal into a two-dimensional function of time and frequency. The precision of this information is limited and depends on the size of the window. Furthermore, once a particular window is chosen, it remains the same for all frequencies.[15]

Recent developments in wavelet theory provide a promising alternative to Gabor transforms: 1) wavelet transforms cover the complete frequency plane, 2) fast algorithms are readily available,

3) wavelet-based feature extraction may be more efficiently incorporated into an image processing system. Wavelet analysis is capable of revealing aspects of data that other signal analysis techniques lack, such as trends, breakdown points, and discontinuities in higher derivatives and self-similarity.[25] The wavelet transforms contain not just the frequency information but spatial information as well. To satisfy the conditions for a wavelet transform, the filter must be a perfect reconstruction filter, that is, the distortion introduced by the forward transform will be canceled in the inverse transform.

Wavelets are functions generated from one single function, the mother wavelet ψ by dilation and translation. Grossmann and Morlet[26] introduced this function ψ, which dilated by a scaling factor and translated by b, enables the analysis, processing, and synthesis of a signal:

$$\psi_{a,b}(x) = |a|^{-\frac{1}{2}}\psi[(a-b)/a], \qquad (a,b) \in R^2, \qquad a \neq 0 \quad (3)$$

We assume x is a one-dimensional variable. The mother wavelet ψ has to satisfy the following admissibility condition:

$$\int \frac{|\Psi(\omega)|^2}{|\omega|}\,\mathrm{d}\omega < \infty$$

where Ψ denotes Fourier transform of ψ. Moreover, if ψ has sufficient decay, then Eq. (3) is equivalent to

$$\int_{-\infty}^{+\infty} \psi(x)\,\mathrm{d}x = 0 \qquad (4)$$

which means that the wavelet ψ exhibits at least a few oscillations and that there is a large choice of functions for ψ.

The basic idea of the wavelet transform is to represent any arbitrary function f as a superposition of wavelets. In practice, it is preferable to express f as a discrete sum rather than as an integral. The coefficients a and b are, thus, discretized such that

$$a = a_0^m, \qquad b = nb_0a_0^m \qquad \text{with} \qquad (m,n) \in Z$$
$$a_0 > 1, \qquad b_0 > 0$$

The wavelet is then defined as

$$\psi_{m,n}(x) = \psi_{a_0^m, nb_0a_0^m}(x) = a_0^{-m/2}\psi\left(a_0^{-m}x - nb_0\right) \qquad (5)$$

and the wavelet decomposition of f becomes

$$f = \sum_{m,n} c_{m,n}(f)\psi_{m,n} \qquad (6)$$

For large, positive values of m ($a > 1$), the ψ function is highly dilated, and large values for the translation step b are well adapted to this dilation. This corresponds to low frequency or narrowband wavelets. For large values of m ($a < 1$), the ψ function is highly concentrated, and the translation step b takes small values. These functions correspond to high frequency or wideband wavelets.[27]

For $a_0 = 2$ and $b_0 = 1$, the functions $\psi_{m,n}$ make up an orthogonal basis belonging to $L2(R)$, where

$$\psi_{m,n}(x) = 2^{-m/2}\psi(2^{-m}x - n), \qquad (m,n) \in Z^2 \qquad (7)$$

The wavelet coefficients $c_{m,n}(f)$ are determined using the relation

$$\psi_{m,n}(x) = \langle f, \psi_{m,n}\rangle = \int f(x)\bar{\psi}_{m,n}(x)\,\mathrm{d}x \qquad (8)$$

A number of filters are available to implement the wavelet transforms. The Harr basis vectors (see Ref. 28) are the simplest and are as follows:

$$\text{low pass: } \left(1/\sqrt{2}\right)[1,1], \qquad \text{high pass: } \left(1/\sqrt{2}\right)[1,-1]$$

A low-pass filter is used to remove the high-frequency information, whereas, a high-pass filter removes low-frequency information. The wavelet transform breaks the image down into four subsampled images. The results consist of the first image, high-pass filtered in both directions; second image, high-pass filtered in the vertical and low-pass filtered in the horizontal direction; third image, low passed in the vertical and high passed in the horizontal direction; and the final image, low-pass filtered in both directions. The convention for displaying the resulting images is given as

Low/Low	Low/High
High/Low	High/High

The computational method known as convolution used in this process is explained briefly next.

Convolution

The process of convolution involves overlaying a mask/filter (basically, a matrix) on the image and multiplying the coincident values and, finally, summing all of the results. This is equivalent to finding the vector inner product of the mask with the underlying subimage.[29] The output image is placed in a separate image array so that the existing values are not overwritten during the process. If the convolution mask is represented as $M(r,c)$ and the image matrix as $I(r,c)$, the process of convolution is given by

$$\sum_{x=-\infty}^{\infty}\sum_{y=-\infty}^{\infty} I(r-x, c-y)M(x,y) \qquad (9)$$

This process can be summarized by the following steps:

1) Convolve the low-pass filters with the rows.

2) Convolve the low-pass filter with the columns of results from step 1, and subsample this result. This gives low/low version of image.

3) Convolve the results from step 1 with high-pass filter on the columns. Subsample the result to produce low/high version of the image.

4) Convolve the original image with the high-pass filter on the rows.

5) Convolve the results of step 4 with low-pass filter on the columns; subsampling yields a high-pass/low-pass version of the image.

6) The high-pass/high-pass version is obtained by convolving the result of step with a high-pass filter on the columns.

The wavelet transform can again be applied to the resulting images, and this process of applying the wavelet transform to resulting images is called multiresolution decomposition. One can compute a wavelet transform of the filtered images and continue recursively to lower resolutions. A predetermined threshold in local energy (strength of the signal) or some other feature can be used to terminate the recursive process.[29]

The images that are obtained using the NDI techniques are resized such that the length and breadth of each image is a power of two because we require the input image to the wavelet transforms to be on a dyadic scale. Once the wavelet transforms are applied, we obtain four images, each of which is one-fourth the size of the original image. All four images are then resized to the original image size. By resizing each of the resulting images, there exists a wavelet coefficient corresponding to every pixel in the original image. The local energy at every pixel location for every image is calculated using a 5×5 Gaussian window. This local energy calculated for each coefficient in the wavelet transformed images for each corresponding pixel forms the feature vector for that particular pixel. This feature vector is used to form clusters and, hence, segment the image.

Clustering Using *K*-Means Algorithm

The feature vector for each pixel from the segmented NDI image serve as an n-dimensional feature vector representing a point within an n-dimensional Euclidean space. The dimensionality depends on the number of levels of wavelet transformations performed. A number of clustering techniques exist that can be used to establish a measure of similarity between pattern vectors. K-means algorithm is one such clustering technique that clusters based on minimum distance.[30]

The input vector formed by the features is of the form, $\boldsymbol{x} = [x_1, x_2, x_3, \ldots, x_n]$. The Euclidean distance between two vectors within the pattern space is given by

$$\|x - z\| = \left[\sum (x_i - z_j)^2 \right]^{\frac{1}{2}} \tag{10}$$

where $\boldsymbol{x}$ and $\boldsymbol{z}$ are the vectors of order n.

The number of cluster centers would be decided based on the number of levels (for example, k) to which we want to segment the image. Once the number of clusters is decided, the first k vectors of the feature vectors can be taken as the initial centers of the k clusters. The K-means algorithm is modified and implemented as follows:

1) The first k vectors are initialized as the centers of the k clusters.

2) Every other vector is read, and its Euclidean distance to the center of the closest cluster to it is calculated and is called NewDis. The Euclidean distance between the closest centers is calculated and is called CenDis.

3) If (NewDis < CenDis), the current vector is classified into its closest cluster and the cluster's center modified accordingly.

4) If (NewDis > CenDis), the two closest clusters are clubbed and the combined center calculated. The current vector is denoted as a new center for a cluster.

The process just explained is repeated until the number of times a new center is formed comes to a steady state. The vector file is then read again to classify each of the vectors to a certain cluster. Because each of the vectors represents a pixel in the original image, every pixel is now classified into one of the k clusters. The average pixel value of each of the clusters is calculated, and all of the pixels belonging to the same cluster are assigned the average value. Once the clusters are formed, two neighboring pixels falls into the same segment if they are in the same cluster. We, therefore, obtain a segmented image that is segmented to k levels, and each cluster would represent one color.

The selection of number of colors for segmentation has a significant impact on the difficulty of feature identification task. If proper number of colors is selected for a specific feature, it can make the feature identification process relatively simple.[28] The problem of determining the true number of clusters has been called the fundamental problem of cluster validity.[31] This is particularly important in image segmentation, where the number of categories is not known a priori.

Classification of Corroded and Noncorroded Regions

Once the image is segmented to a certain number of levels, the next task is to distinguish the segments that represent the corroded regions from those which represent the noncorroded regions. A wide variety of features can be extracted from each of the segments and can be used to identify the damaged regions. Binary object features such as area of each segment, perimeter, thinness ratio, and aspect ratio can be calculated. The histogram features can include the mean of the pixel values in the segment, standard deviation, skew, energy, and entropy.[28] These features form the feature vector for classifying between the corroded and uncorroded regions. Because the number of segments that were formed is usually very high, only mean and standard deviation using the low-pass/low-pass wavelet coefficients were used.

The classification process is based on K-means clustering algorithm. It involves a training phase and a testing phase. In the training phase, few images of damaged panels were taken and segmented using the segmentation algorithm described earlier. Segments that represented regions of corrosion were identified manually, and the feature vector was formed for each segment. A flag representing corrosion or no corrosion was also added to the feature vector. The K-means classifier was then used to classify the feature vectors. The knowledge of the K-mean classifier is stored by maintaining the values of the cluster centers for each cluster. The cluster that contains the maximum number of segments that hold the flag representing corrosion is marked as a cluster representing damaged regions.

In the testing phase, images of the damaged panels were segmented, and features were extracted from each segment. The resulting feature vector is classified into one of the two clusters formed during the training phase. If the feature vector is classified into a cluster that was marked corroded, the segment representing it is identified as a damaged region.

IV. Damage Quantification

Once the damaged regions are identified on the image, the next task is to quantify these damages following the process shown in Fig. 3. The extent of material loss is used to quantify the damages on the panels. Various features that were obtained on the corroded region based on histogram and/or wavelet analysis during the segmentation stage are used to estimate the material loss.

First-order statistical features of the identified segments are computed using the histogram of the NDI images. These first-order features include 1) mean, 2) standard deviation, 3) skew, 4) energy, and 5) entropy. The first-order histogram probability $P(g)$ is defined as $P(g) = N(g)/M$, where M is the number of pixels in the image and $N(g)$ is the number of pixels at gray level[29] g. Then, the first-order features are calculated as follows:

1) For the mean, the average value is defined as

$$\bar{g} = \sum_{g=0}^{L-1} gP(g) = \sum_r \sum_c \frac{I(r,c)}{M}$$

2) The standard deviation is defined as

$$\sigma_g = \sqrt{\sum_{g=0}^{L-1} (g - \bar{g})^2 P(g)}$$

3) The skew measuring the asymmetry is

$$\frac{1}{\sigma_g^3} \sum_{g=0}^{L-1} (g - \bar{g})^3 P(g)$$

4) The energy is

$$\text{energy} = \sum_{g=0}^{L-1} [P(g)]^2$$

5) The entropy is

$$\text{entropy} = -\sum_{g=0}^{L-1} P(g) \log_2 [P(g)]$$

The second-order features are calculated using a cooccurance matrix. The cooccurance matrix is an estimate of the second-order joint probability density. The joint probability is $P(i, j, d, t)$, the probability of gray levels i and j occurring at distance d and angle t. A cooccurance matrix for distance d and angle t is composed of elements g_{ij}, which record the number of pixel pairs d units apart in the direction t, with one gray level at i and one at j, the order being immaterial. The cooccurance matrix is used to calculate the second-order features as follows.

Angular second moment (ASM):

$$\text{ASM} = \sum_i \sum_j [g(i, j)]^2$$

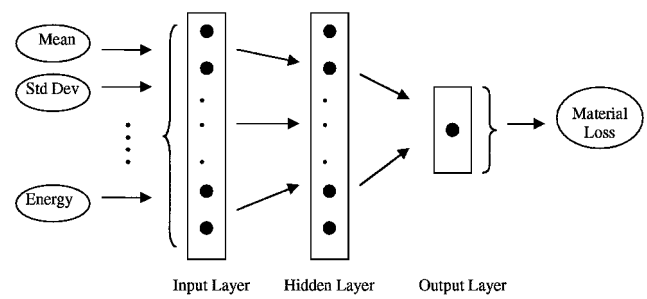

Fig. 3 Overall organization of the backpropagation NN showing the input/output features used.

Inverse difference moment (IDM):

$$\text{IDM} = \sum_i \sum_j \frac{1}{(j-i)^2} g(i, j)$$

Entropy:

$$\text{entropy} = \sum_i \sum_j g(i, j) \log[g(i, j)]$$

Contrast:

$$\text{contrast} = \sum_i \sum_j (i-j)^2 g(i, j)$$

An artificial neural network (ANN) is used for the prediction of material loss using the first- and second-order features. ANNs are capable of realizing a variety of nonlinear relationships of considerable complexity.[12] Pidaparti and Palakal[32] have successfully investigated the fatigue life and crack growth using neural networks. The ANN used for predicting material loss has input nodes equal to the number of features extracted from each segment. Figure 3 shows the overall architecture of the backpropagation neural network that is used in this study. The number of input nodes used is based on the number of features considered. Because the NDI images are in color, there are three components, red, green, and blue, for each feature. Experiments were conducted using 6 (mean and standard deviation 3 times), 15 (five first-order features 3 times) and 27 (five-order features plus four second-order features 3 times) inputs features. There is only one output node for the network indicating the material loss in the segment to which the feature vector corresponds. The set of weights is initially assigned randomly. The training of the network involves adjusting the weights to reduce the error within some predefined limit. After a good number of training examples, the network would then be used to predict the material loss due to corrosion.

V. Experimental Results

Damage Identification

Experiments are conducted on the corroded images obtained from the FAA–NDI Validation Center, Albuquerque, New Mexico. A set of damaged aircraft panels with corrosion obtained using eddy-current NDI technique were used for damage identification experiments. For damage quantification experiments, five different data sets that were obtained using ultrasound NDI on specimens with engineered corrosion were used, as shown in Table 1. For each set, 10 different specimens, labeled P–Y, were used for which the material loss is known.

A sample image panel with corrosion taken using eddy current at 5 kHz is shown in Fig. 4a. The image in Fig. 4a has four darker regions representing the corroded areas. The first step is to segment the image to isolate these regions from the rest of the image. The original image was, therefore, segmented using wavelet transforms and clustering techniques as described in Sec. III. The image was segmented to four clusters, shown in Fig. 4b. It can be clearly observed that the damaged regions have been isolated from the rest of the image shown as dark regions in Fig. 4b.

Features extracted from two panels obtained using eddy current at 5 kHz were used to form four clusters. Four clusters were chosen empirically: Fewer than four clusters resulted in poor classification results, whereas more than four clusters did not improve the classification performance. The number of clusters determines the number of levels (colors) to which each image would be segmented.

Table 1 Set of specimens and their description used in the damage quantification study

Set no.	Specimen set	Description
1	DC 91	15% material loss
2	DC 92	20% material loss
3	DC 93	5% material loss
4	DC 94	10% material loss
5	DC 95	25% material loss

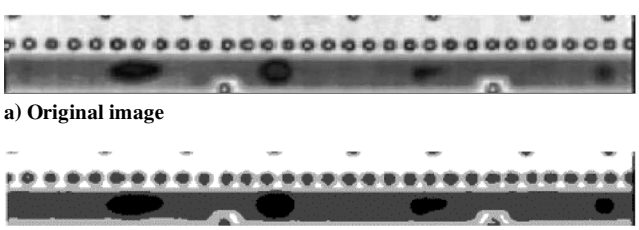

a) Original image

b) Identified image showing corroded segments

Fig. 4 Results of corrosion damage identification process.

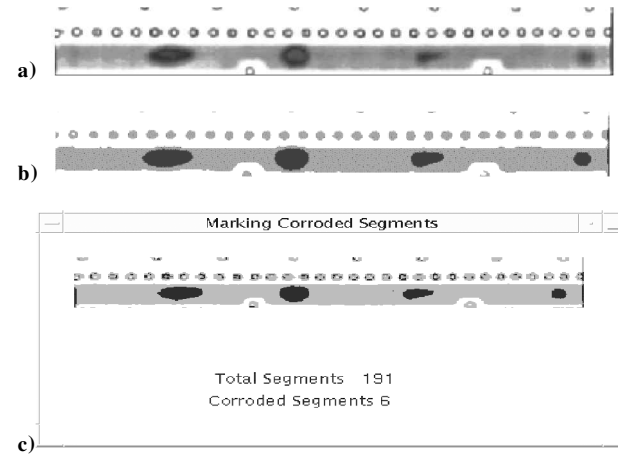

Fig. 5 Segments identified as damaged regions.

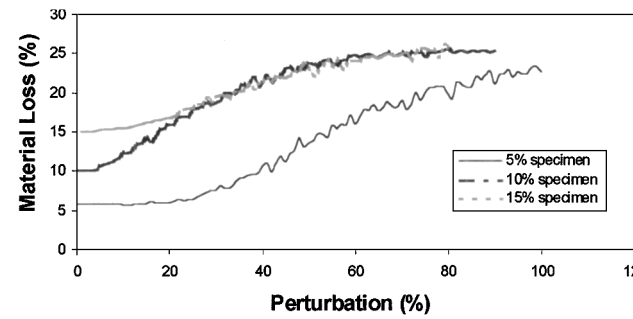

Fig. 6 Effect of perturbing the original damage image on material loss on three different specimens.

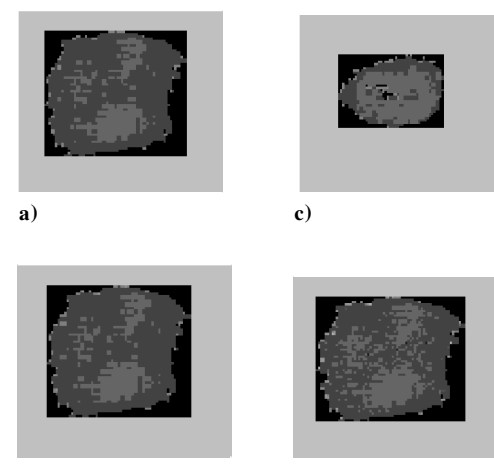

Fig. 7 Comparison of simulated damage images with original damage images: a) original 15% material loss region, b) 15% material loss image with 20% perturbation, c) original 20% material loss region, and d) 15% material loss image with 40% perturbation.

Each segment was isolated, and the feature vector was formed with the extracted features as explained earlier. The segments that were known to represent the corroded regions were marked whereas the rest of the segments representing the undamaged regions were not marked. Clusters were then formed using all of the feature vectors. After the clusters were formed, one of the clusters was marked as a corroded cluster because it was formed by the majority of the vectors representing the corroded segments.

For the identification of damaged regions, the feature vector from each segment was now classified into the clusters formed during the training phase. If the feature vector was classified into a cluster that was marked corroded, the segment from which the vector was formed is identified as the corroded region.

Figure 5 shows the screen showing the panel from Fig. 4, when tested to identify the damaged regions. The panel was initially segmented into 191 segments consisting of both corroded and noncorroded regions, and features were extracted from each segment. The 191 segments were automatically identified based on the intensity and color changes detected by the wavelet algorithm. These feature vectors were then classified into corroded or noncorroded segments. A total of 6 out of 191 segments were identified as damaged regions, as shown in Fig. 5.

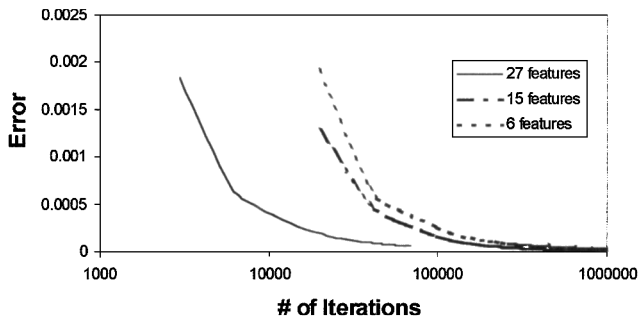

Fig. 8 Comparison of error curve for three different backpropagation networks used during the training stage.

Damage Quantification

Experiments for quantification of corrosion damage were conducted on NDI images with the specimen set given in Table 1. Because the corrosion was engineered on these specimens, the extent of material loss on each specimen was known. Images of each of these specimens were segmented, and the corroded region was isolated. The damage quantification is estimated using the ANNs based on various features obtained from these corroded regions. For the neural network to learn and generalize properly, a large set of data is necessary. However, the number of specimens available and the corroded regions obtained from these specimens were small. Therefore, a large simulated data set was created by perturbing the original corroded regions. This process is described next.

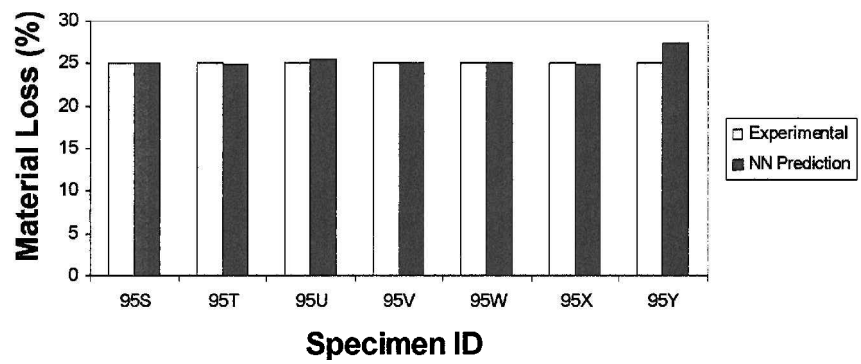

a) For specimen set 95

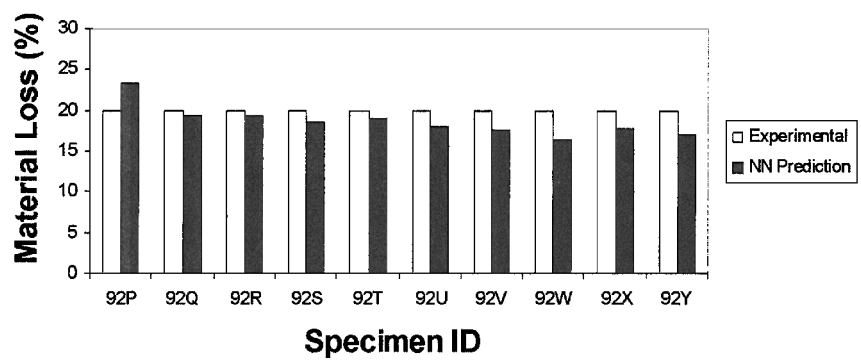

b) For specimen set 92

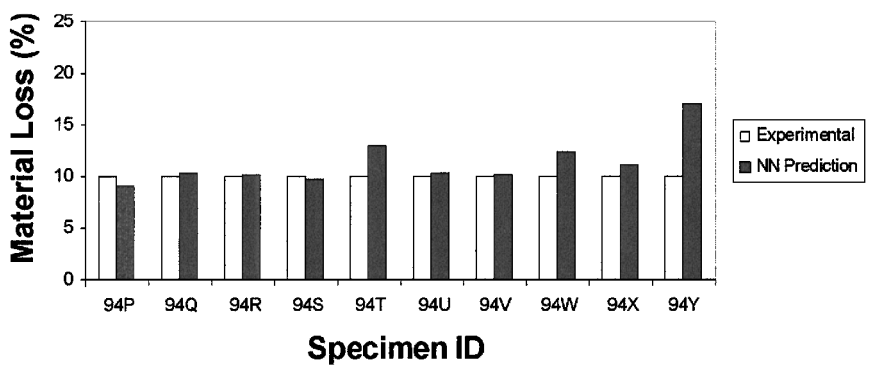

c) For specimen set 94

Fig. 9 Comparison of NN predicted material loss with the experimental data for three sets of specimens shown in Table 1.

Simulated Data

The original corroded regions were perturbed by the adding random noise to the red, green, and blue intensities. The images were perturbed so that they would indicate a growth in corrosion. At each step the value of the random number added was increased, and the material loss was compared against known corroded regions.

A steady growth in corrosion of the specimens due to higher perturbation is shown in Fig. 6. The three curves in Fig. 6 indicate the material loss for the original 5, 10, and 15% material loss specimens. When the images were not perturbed, the material loss obtained was close to the actual material loss values for these specimens. When the images were perturbed in the direction of growth in corrosion, all three curves showed a gradual increase in the material loss. For example, a 15% material loss region with 40% perturbation resulted in 20% material loss, which is comparable to the actual 20% material loss region. This can be clearly seen in Fig. 6.

Figure 7 further shows the validity of using the perturbed images for the corrosion quantification study. Figures 7a and 7c are original damaged regions with 15 and 20% material loss, respectively. The 15% region (Fig. 7a) was perturbed to 20 and 40%. The 40% perturbation resulted in a 20% material loss, which was comparable to the 20% material loss region in Fig. 7c. The perturbed images, therefore, provided an alternative to obtain a large set of data required for the neural network training. It also allowed observation of how corrosion would grow at the pixel level over a period of time.

Neural Network Training for Damage Estimation

For the neural network training and prediction, five images from each specimen listed in Table 1, giving a total of 25 images, were used. These NDI images from various specimens provided the corroded regions. When these corroded regions were used, 1×10^5 segments were generated for the 6-feature experiment and 1×10^6 segments were generated for the 15 and 27 feature experiments, using the perturbation process. From these regions, the first- and second-order features were obtained for the neural network training.

The learning parameters used for network were learning rate 0.25, momentum factor 0.9, and gain factor 1.0. Experiments with the first-order features used a network of size $6 \times 4 \times 3 \times 1$ (6 input nodes, 2 hidden layers with 4 and 3 hidden nodes each, and 1 output node). The input features (mean and standard deviation for red, green, and blue colors of the images) were used. The network was trained with first-order features obtained from simulated corroded regions. A second network of size $15 \times 10 \times 4 \times 1$ (15 input nodes, 2 hidden layers with 10 and 4 hidden nodes, and 1 output node, respectively) was trained with 15 second-order features (mean, standard deviation, energy, entropy, inertia, etc.). This network was also trained with features obtained from simulated corroded regions. A third network of size $27 \times 15 \times 5 \times 1$ (27 input nodes and 2 hidden layers with 15 and 5 hidden nodes, and 1 output node) with third-order features consisting of 27 features was trained using features obtained from simulated images. Figure 8 shows the absolute error for all three networks. All three networks converged to an acceptable level, however; the 27-feature network took a long time to converge.

Damage Prediction Using Neural Networks

The features extracted from the original damaged regions obtained from the specimens shown in Table 1 was used to test the network and, hence, to predict the material loss. All three networks

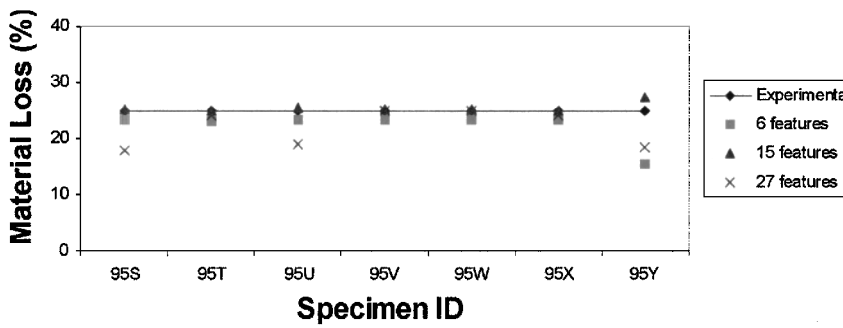

a) For specimen set 95

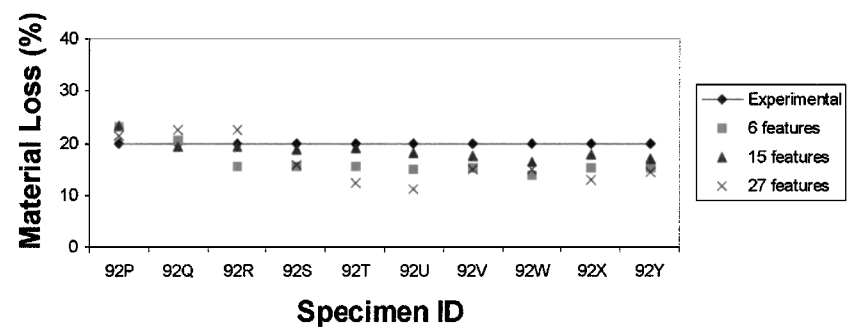

b) For specimen set 92

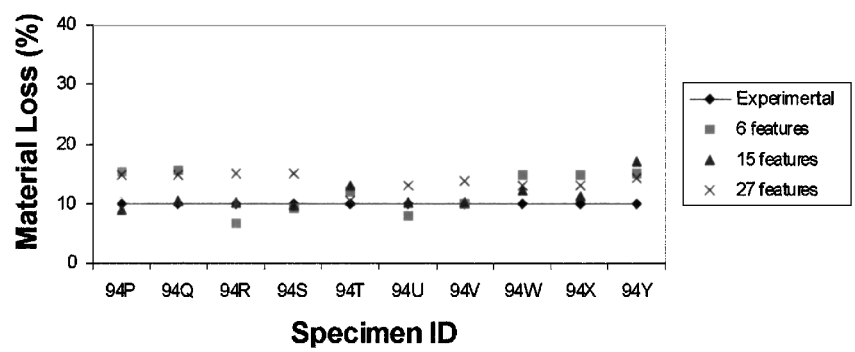

c) For specimen set 94

Fig. 10 Comparison of material loss predictions using various number of wavelet features for three sets of different specimens shown in Table 1.

were used to predict the material loss, and the results shows the effect of the number features needed for accurately predicting the damage.

The results given in Figs. 9a–9c show the actual material loss and the neural network prediction for the second-order feature network (network trained with 15 features) for three sets of specimens 95, 92, and 94. These results indicate that the material loss of a specimen can be predicted reasonably well using the second-order features by the neural network.

To see how the wavelet features affect the material loss predictions, a number of experiments were conducted and presented in Fig. 10. The material loss prediction by the network is compared with the original data. Figure 10 shows the neural network (NN) performance for all three networks for specimens 95, 92, and 94. It can be observed that the results obtained using 15 features yielded better performance than that obtained using 6 and 27 features. These results show that lower-order features are not sufficient to capture the necessary information for predicting the material loss. On the other hand, the second-order features were subjected to noise from surrounding regions close to the corroded region, thus resulting in poor material loss prediction.

VI. Conclusions

An intelligent computational approach based on wavelet analysis and ANNs was developed to identify and quantify the corrosion damage images on panels obtained from NDI techniques. Wavelet transforms using the Harr filter have been used for extracting parameters that were used for segmenting the image. A K-means classification algorithm was used to identify the corroded regions from the noncorroded regions in the panel based on the extracted features. Good accuracy was obtained in identification of the corroded segments. A backpropagation NN was used to predict material loss due to corrosion. Perturbing the images by changing the pixel values that would correspond to the higher material loss due to growth in corrosion was simulated. Experiments were conducted by perturbing the images of the damaged regions such that growth in the extent of material loss can be observed. A good trend was observed between the predicted material loss and the experimental data. The results presented indicate that the computational methods developed for corrosion analysis seem to provide reasonable results for estimating material loss due to corrosion damage. Further research is being conducted to develop an integrated structural damage assessment system to estimate the severity of damage in aging structures and materials.

Acknowledgments

The authors would like to thank the National Science Foundation for supporting this work under Grant CMS-9812723. We would also like to thank T. P. Sivam and Shannon Mason of Ratheyon for providing the images/data that were required to conduct the experiments.

References

[1]Doctor, P. G., and Harrington, T. P., "Analysis of Eddy Current Data Using Pattern Recognition Methods," *Proceedings of the IEEE 5th International Joint Conference on Pattern Recognition*, Inst. of Electrical and Electronics Engineers, New York, 1980, pp. 137–139.

[2]Shanker, R., "Feasibility of Using Adaptive Learning Methods for Eddy Current Signal Analysis," Electric Power Research Inst., Rept. EPRI NP-723, TPS77-723, Palo Alto, CA, March 1978.

[3]Elsley, R. K., and Graham, L. J., "Pattern Recognition Techniques Applied to Sorting Acoustic Emission Signals," *IEEE Ultrasonic Symposium Proceedings*, Inst. of Electrical and Electronics Engineers, New York, 1976, pp. 147–150.

[4]Chan, W. Y., Hay, D. R., Suen, C. Y., and Schwelb, O., "Application of Pattern Recognition Techniques in the Identification of Acoustic Signals," *Proceedings of the IEEE 5th International Joint Conference of Pattern Recognition*, Inst. of Electrical and Electronics Engineers, New York, pp. 108–111.

[5]Chen, C. H., "On High Resolution Ultrasonic Inspection System," *Review of Progress in Quantitative Nondestructive Evaluation*, edited by D. O. Thompson and D. E. Chimenti, Vol. 9A, Plenum, New York, 1990, pp. 959–965.

[6]Hay, D. R., "ICEPAK (Intelligent Classifier Engineering Package) Pattern Recognition Software Package," Tektrend International, Inc., Montreal, QC, Canada, 1989.

[7]Mucciardi, A. N., "TestPro Software Package," Infometics, 1987.

[8]Chen, C. H., "Pattern Recognition in Nondestructive Evaluation of Materials," *Handbook of Pattern Recognition and Computer Vision*, World Scientific, 1993, pp. 455–472.

[9]Upda, L., and Upda, S. S., "Eddy Current Defect Characterization Using Neural Networks," *Material Evaluation*, Vol. 48, 1990, pp. 342–353.

[10]Chen, C. H., Pau, L. F., and Wang, P. S. P. (eds.), *Handbook of Pattern Recognition and Computer Vision*, World Scientific, River Edge, NJ, 1992, pp. 235–276.

[11]Levens, S., "Image Analysis for Material Characterization," Univ. Antwerpen, Antwerpen, The Netherlands, 1998.

[12]Masters, T., *Practical Neural Network Recipes in C++*, Academic Press, London, 1993.

[13]Unser, M., and Eden, M., "Multiresolution Feature Extraction and Selection for Texture Segmentation," *IEEE Transactions on Pattern Analysis and Machine Intelligence*, Vol. 11, No. 7, 1989, pp. 717–728.

[14]Unser, M., "Texture Classification and Segmentation Using Wavelet Frames," *IEEE Transactions on Image Processing*, Vol. 4, No. 11, 1995, pp. 1549–1560.

[15]Laine, A., and Fan, J., "An Adaptive Approach for Texture Segmentation by Multi-Channel Wavelet Frames," Center for Computer Vision and Visualization, Univ. of Florida, Gainesville, FL, 1993.

[16]Jain, A. K., and Dubuisson, M. P., "Segmentation of X-Ray and C-Scan Images of Fiber Reinforced Composite Materials," *Pattern Recognition*, Vol. 25, 1992, pp. 257–270.

[17]Smith, F. G., Jepsen, K. R., and Lichtenwalner, P. F., "Comparison of Neural Network and Markov Random Field Image Segmentation Techniques," *Review of Progress in Quantitative Nondestructive Evaluation*, edited by D. O. Thompson and D. E. Chimenti, Vol. 11A, Plenum, New York, 1992, pp. 717–724.

[18]Tuceryan, M., and Jain, A. K., "Texture Analysis," *Handbook of Pattern Recognition and Computer Vision*, edited by C. H. Chen, L. F. Pau, and P. S. P. Wang, World Scientific, River Edge, NJ, 1992, pp. 235–276.

[19]Gibson, J. J., *The Perception of the Visual World*, Houghton Mifflin, Boston, MA, 1950.

[20]Tuceryan, M., and Jain, A. K., "Texture Segmentation Using Voronoi Polygons," *IEEE Transactions on Pattern Analysis and Machine Intelligence*, Vol. 12, 1990, pp. 211–216.

[21]Cochen, F. S., and Cooper, D. B., "Simple Parallel Hierarchical and Relaxation Algorithms for Segmenting Noncausual Markovian Random Fields," *IEEE Transactions on Pattern Analysis and Machine Intelligence*, Vol. 9, 1987, pp. 195–219.

[22]Therrien, C. W., "An Estimation-Theoretic Approach to Terrain Image Segmentation," *Computer Vision, Graphics and Image Processing*, Vol. 22, 1983, pp. 313–326.

[23]Malik, J., and Perona, P., "Preattentive Texture Discrimination with Early Vision Mechanisms," *Journal of the Optical Society of America*, Series A, Vol. 7, 1990, pp. 923–932.

[24]Turner, M. R., "Texture Discrimination by Gabor Functions," *Biological Cybernetics*, Vol. 55, 1986, pp. 71–82.

[25]Mistiti, M., Misiti, Y., Oppenheim, G., and Poggi, J., "Wavelet Toolbox, for use with MATLAB," MathWorks, Natick, MA, 1996.

[26]Grossmann, A., and Morlet, J., "Decomposition of Functions into Wavelets of Constant Shape, and Related Transforms," *Mathematics and Physics*: *Lectures on Recent Studies*, edited by L. Striet, World Scientific, Singapore, 1985.

[27]Daubechies, I., "Ten Lectures on Wavelets," *CBMS-NSF Regional Conference Series in Applied Mathematics*, Society for Industrial and Applied Mathematics, Philadelphia, 1995.

[28]Umbaugh, S., "Computer Vision and Image Processing," *A Practical Approach Using CVIP Tools*, Prentice–Hall, Upper Saddle River, NJ, 1998.

[29]Fatemi-Ghomi, N., Palmer, P. L., and Petrou, M., "Performance of Texture Segmentation Algorithms Based on Wavelets," Dept. of Electronics and Electrical Engineering, Univ. of Surrey, Surrey, England, U.K., 1995.

[30]Pandya, S., and Macy, R. B., *Pattern Recognition with Neural Networks in C++*, CRC Press, Boca Raton, FL, 1996.

[31]Dubes, R., "Cluster Analysis and Related Issues," *Handbook of Pattern Recognition and Computer Vision*, edited by C. H. Chen, L. F. Pau, and P. S. P. Wang, World Scientific, 1993, pp. 3–32.

[32]Pidaparti, R. M. V., and Palakal, M., "Fatigue Crack-Growth Prediction of Multiple Site Damage Panels Using Neural Network Models," *Journal of Aircraft*, Vol. 36, No. 7, 1998, pp. 1300–1304.

S. Saigal
Associate Editor